Li Deintercalation and Structural Change in the Lithium Transition Metal Nitride Li$_3$FeN$_2$

M. Nishijima, Y. Takeda,[1] N. Imanishi, and O. Yamamoto

Department of Chemistry, Faculty of Engineering, Mie University, Kamihama-cho 1515, Tsu, Mie-ken 514, Japan

and

M. Takano

Institute for Chemical Research, Kyoto University, Uji, Kyoto-fu 611, Japan

Li$_3$FeN$_2$ with a non-dimensional structure was prepared by heating a mixture of Li$_3$N and Fe$_4$N in a 1% H$_2$–99% N$_2$ gas stream. Li ion was easily deintercalated, forming Li$_{3-x}$FeN$_2$ in a range of $0 \leq x \leq 1.0$ in a Li/Li$_3$FeN$_2$ cell. With increasing x, four kinds of phases having orthorhombic symmetry appeared sequentially. Electrical resistivity decreased with increasing x. Mössbauer spectra suggested that Li deintercalation oxidizes Fe(III) to Fe(IV). The Li/Li$_3$FeN$_2$ cell showed a good reversibility, with a high current density (500 μA cm^{-2}). Li$_3$FeN$_2$ is thus believed to be a good candidate for an electrode for lithium secondary batteries. © 1994 Academic Press, Inc.

INTRODUCTION

It is well known that Li$_3$N has a high Li ion conductivity of about 1×10^{-2} S cm^{-1} at room temperature. Numerous studies of this interesting material as a solid electrolyte have been performed in the past 10 years (1–3). However, Li$_3$N has a lower decomposition voltage (0.44 V), which makes it difficult to be used as an electrolyte for solid lithium batteries.

In the system Li–metal–nitrogen, a series of nitrides with a general composition Li$_{2n-1}$MN$_n$ (M, some elements of groups 3 and 4 and some transition metals; $n = 2, 3$) has been known for a long time (4–6). These nitrides crystallize in the antifluorite-type structure (5), where Li ions occupy the positions of fluorine in CaF$_2$. As the fluorite structure has a larger lattice energy, these nitrides may be expected to be very stable. In addition, it is known that Li–nitrides with 3rd and 4th group metals such as Li$_3$BN$_2$ (7, 8), Li$_3$AlN$_2$ (9), and Li$_5$SiN$_3$ (10) exhibit high ionic conductivity; their structural and electrical proper-

ties have, therefore, been extensively studied as a solid electrolyte for solid Li secondary batteries.

Studies of Li$_{2n-1}$MN$_n$ containing transition metals such as Mn (11), Fe (12), etc., have also been carried out, but these did not deal with the electrochemical properties of these interesting compounds. The introduction of transition metals might produce conduction electrons which spoil their properties as an electrolyte. This disadvantage could be turned into an advantage if the material is useful as an electrode for lithium secondary batteries. Possibly, the high lithium ion mobility originating in the fluorite structure and the low reduction or oxidation potentials of transition metals facilitate Li deintercalation and subsequent Li intercalation in these nitrides. If such reversibility can be realized, Li$_{2n-1}$MN$_n$ would be good not only as a candidate electrode for Li secondary batteries, but also for exotic materials containing transition metals in unusual oxidation states such as Fe^{4+} and Co^{4+}, which cannot be prepared by other methods.

We tried to prepare this type of nitride by first reacting transition metal nitrides M_xN$_y$ (M = Ti, V, Cr, Mn, Fe, Co, Ni, or Cu) and a lithium nitride Li$_3$N. We found that Li$_3$FeN$_2$ could be easily synthesized, using a traditional ceramic method in a 1% H$_2$–99% N$_2$ stream: the resulting material showed extremely smooth Li deintercalation and intercalation.

EXPERIMENTAL

Li$_3$N and Fe$_4$N (kindly offered by Nihon-shin-kinzolu Co. Ltd.) were used as raw materials. Li$_3$N was prepared by a reaction of extrapure lithium sheets and nitrogen at temperatures between 80 and 150°C in a glass reactor; the product formation was confirmed by X-ray diffraction (XRD) measurements and also by weight increase. Mixtures of Li$_3$N and Fe$_4$N were pressed into tablets 8 mm

---

[1] To whom correspondence should be addressed.

in diameter and 5–8 mm in thickness under a pressure of 3 MPa; these were subsequently heated in an electrical furnace at 600°C for 12 hr in a 1% H_2–99% N_2 stream. The heating rate was 10°C/min. Before firing, the furnace was evacuated with a rotary pump to remove moisture, oxygen, and CO_2. Powder XRD measurements were performed on a Rigaku RAD-RC (12 kW) using monochromatic Cu$K\alpha$ radiation. As the products were very hygroscopic, they were protected against moisture during the XRD measurement by using a gas-tight holder filled with argon gas. A 7-μm thick aluminum window covered the sample holder plate in an arc.

For the electrochemical study we aimed at obtaining $Li_{3-x}FeN_2$ having various x values. Single-phase Li_3FeN_2 was ground and mixed with acetylene-black (electron conductor) and Teflon (binder), and the mixture was pressed into a tablet 12 mm in diameter under a pressure of 1 MPa. A conventional Li-coin-type cell was assembled using this tablet as a cathode, a Li sheet as an anode, and $LiClO_4$/PC + DME as an electrolyte. Li ion was deintercalated by discharging the cell at 150 μA cm^{-2}.

All the treatments except for heating in a furnace and the discharge–charge experiments were carried out in an Ar-filled dry box.

Samples with different Li content were investigated by XRD. For a Rietveld analysis the intensity data were collected at each 0.02° step width for 2 or 3 sec over a 2θ range from 10 to 100°. A computer program (REITAN) was used for a profile refinement calculation (13). The electrical resistivity of $Li_{3-x}FeN_2$ ($0 \le x \le 1$) was measured by a four-probe method in a temperature range between 15 and 300 K. ^{57}Fe Mössbauer measurements were performed at room temperature. The ^{57}Co/Rh source velocity was calibrated by using pure iron metal as the standard.

RESULTS AND DISCUSSION

1. Synthesis and Crystal Structure

Gudat *et al.* (12) reported that Li_3FeN_2 was prepared from Fe metal and molten Li in a N_2 stream. This method requires high-purity N_2 gas and a special furnace. As we wanted to use a conventional furnace, we chose Li_3N and Fe_4N as starting materials. We found that Li_3FeN_2 could be easily prepared from mixtures of Fe_4N and Li_3N powder in a 1% H_2–99% N_2 gas stream. When commercial N_2 gas was used, oxides and carbonates formed instead of the nitride, because moisture, oxygen, and CO_2 were present as impurities in the N_2 gas.

Starting mixture ratios, firing conditions, and the resulting phases are listed in Table 1, and the XRD patterns of the products are shown in Fig. 1. Peaks at $2\theta = 30.5°$ (Li-rich side) and 44.5° (Fe-rich side) come from impurity phases. The phase responsible for the peak at $2\theta = 30.5°$

TABLE 1
Reacting Condition and Products in the Li_3N–Fe_4N System

Li:Fe	Rate (°C/min)	Temperature (°C)	Hold (hr)	Products
3.0:1	10	600	12	Li_3FeN_2 + NaCl-type
4.0:1	10	600	12	Li_3FeN_2 + unknown + Li_3N (trace)
5.0:1	10	600	12	Li_3FeN_2 + unknown + Li_3N (trace)
3.5:1	10	500	12	Li_3FeN_2 + unknown + NaCl-type
3.5:1	10	600	12	Li_3FeN_2
3.5:1	10	700	12	Melt
3.5:1	100	600	12	Li_3FeN_2
3.5:1	1	600	12	Li_3FeN_2 + NaCl-type + unknown

is unknown, but the peak at $2\theta = 44.5°$ seems to be associated with a NaCl-type compound. It is clear that the starting molar ratio of 3.5:1 produces single-phase Li_3FeN_2. The XRD pattern agrees with that reported by Gudat *et al.* (12). Excess Li_3N might have evaporated during the reaction. Most lithium-containing nitrides have been prepared from Li-excess mixtures, as reported, for example, by Formont *et al.* (6). The fact that when the heating rate was below 2°C/min, the single phase could not be obtained even if the starting molar ratio was 3.5:1, might have resulted from evaporation during heating. As discussed in the next section, however, we cannot rule out a Fe deficiency such as $Li_3Fe_{1-y}N_2$.

We tried to use Fe metal powder instead of Fe_4N, but no single phase could be obtained under any of the conditions listed in Table 1.
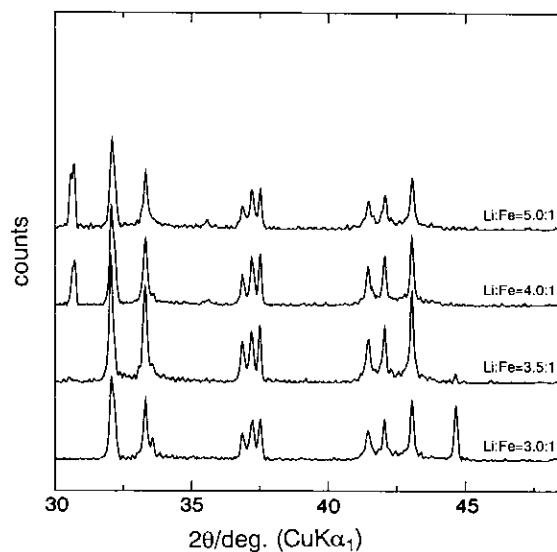

FIG. 1. XRD patterns of the products obtained from various starting compositions.

TABLE 2

Crystallographic Data, Atomic Positions, and Displacement Parameters of Li_3FeN_2

Space group	*Ibam*
Lattice constants (Å)	$a = 4.8630(3)$
	$b = 9.6381(5)$
	$c = 4.7833(2)$
D (g cm⁻³)	2.96

Atom	Wyckoff position	Occupancy	x	y	z	$U_{eq}(pm2)a$
Li(1)	8*j*	1.0000	0.0000	0.7434(6)	0.2500	97(17)
Li(2)	4*b*	1.0000	0.5000	0.0000	0.0000	97(17)
Fe	4*a*	0.356(3)	0.0000	0.0000	0.2500	41(4)
N	8*j*	1.0000	0.2278(2)	0.8783(4)	0.0000	71(13)

Single-phase Li_3FeN_2 assumes orthorhombic symmetry, space group *Ibam*. The crystallographic data from the Reitveld refinement are given in Table 2. As shown in Fig. 2, Li_3FeN_2 crystallizes in a distorted antifluorite structure, in which Fe_4N tetrahedra sharing edges with each other form one-dimensional chains along the c direction.

In the present work, the single phase of Li_3FeN_2 was synthesized from a mixture of Li_3N and Fe_4N at a ratio of Li : Fe = 3.5 : 1, not 3 : 1. As mentioned above, we first thought that the difference between the formal composition and the starting ratio was caused by evaporation of Li_3N during synthesis. Gudat *et al.* (12) also refined the structure by fixing the composition as Li_3FeN_2. But in our structure refinement, fixing of the molar ratio at Li : Fe = 3 : 1 did not result in a reasonable value of the reliability factor (R). When the Fe site occupancy was varied, it converged to 0.86 with a low R factor. This value agrees well with the batch composition (Li : Fe = 3.5 : 1 = 3 : 0.857), which suggests that the Fe sites (4*a*) are relatively vacant, or that a substitution of Li for Fe at the 4*a* site occurs rather than the Li evaporation.
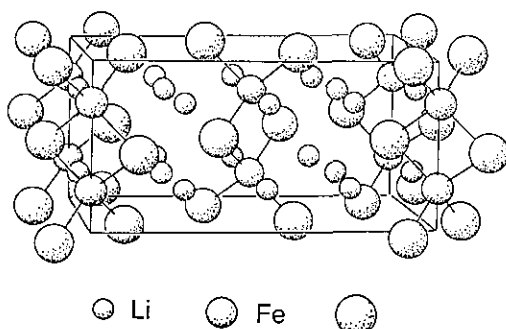
Atomic distances shown in Table 3 agree well with Gudat's data; however, the composition of our sample is most likely different from the ideal one, Li_3FeN_2.

2. Li Deintercalation and Structure Changes

Figure 3 shows the closed-circuit voltage (CCV) and open-circuit voltage (OCV) curves of the Li/Li_3FeN_2 cell for the charge direction (Li deintercalation) at a current density of 150 μA cm⁻². Both the CCV and the OCV are very flat in a wide range (the potential only increases by 30 mV from $x = 0$ to 0.6), and the difference due to an overpotential is very small. These properties of Li_3FeN_2 are very characteristic and remarkable, and these are advantageous for the practical use of this material as an electrode for Li cells.

X-ray diffraction patterns for various Li contents, x, are shown in Fig. 4. The extraction of Li occurs smoothly up to $x = 1.0$; however, in the range of $x > 1.0$, the CCV suddenly increases, and XRD patterns become indistinct. This probably is the result of the decomposition of $Li_{3-x}FeN_2$.

Four distinct phases have been found to form for $x < 1.0$. All these phases have orthorhombic symmetry, *Ibam*. In order of appearance, they are α, β, γ, and δ phases. The lattice parameters of each phase are listed in Table 4, and the variation of these parameters with total Li content is shown in Fig. 5. The volume ratio of these

FIG. 2. Crystal structure of Li_3FeN_2.

TABLE 3

Selected Interatomic Distances (Å)

Fe–N	2.00(2)
Li(1)–N	2.09(4)
	2.13(4)
Li(2)–N	2.13(3)

NISHIJIMA ET AL.

TABLE 4
Lattice Parameters of Each Phase

	a	b	c
a phase	4.8630(3)	9.6318(5)	4.7833(2)
b phase	4.830(3)	9.400(4)	4.714(3)
g phase	4.820(1)	9.100(3)	4.750(2)
d phase	4.915(3)	8.604(7)	4.769(4)

phases was roughly estimated from the peak intensity as a function of total Li content, as shown in Fig. 6. The inhomogeneous reaction in the Li cell sometimes gives rise to a coexistence of the α, β, and γ phases. A typical two-phase reaction seems to occur on Li deintercalation up to $x = 0.75$. For $x < 0.75$ each phase keeps its parameter values almost constant, and each solid solution range seems to be very narrow: that is, $x = 0$ for the α phase, $x = 0.5$ for the β phase, and $x = 0.75$ for the γ phase. The lattice parameters, especially the b axis, decrease sequentially this set of phase transitions.

The phase changes have been considered below based on the OCV, CCV, and XRD results.

(a) α–β ($0 \leq x \leq 0.5$). The change in lattice parameters from the α to the β phase is isotropic, though relatively large. In this stage, the OCV curve is perfectly flat, suggesting that the difference in Gibb's free energy is very low.

(b) β–γ ($0.5 \leq x \leq 0.75$). As for the change from α to β, the a and b parameters decrease, while the c axis increases. Because of the larger change in Gibb's free energy compared to α–β, the OCV has a step in this range.

(c) γ–β ($0.75 \leq x \leq 1.00$). Though there is no change in space group, the a and c axes of the δ phase largely increase and the b axis decreases in comparison with those of phase γ. Phase δ exists as a monophasic solid solution for $0.75 \leq x \leq 1.00$.

As seen in Fig. 5, the b axis monotonically decreases with phase changes from the α phase to the δ phase. This

FIG. 4. X-ray diffraction patterns of $Li_{3-x}FeN_2$ for various charge depths.

indicates that Li is deintercalated from (0 0 4) planes, that is, Li(1) is predominantly deintercalated.

As mentioned above, $Li_{3-x}FeN_2$ decomposes at $1.0 < x$. The decomposition also occurs when the current density is increased. When the overpotential was very high (if the current density was large), decomposition began at smaller x values. The decomposition voltage was estimated to be about 1.5 V.
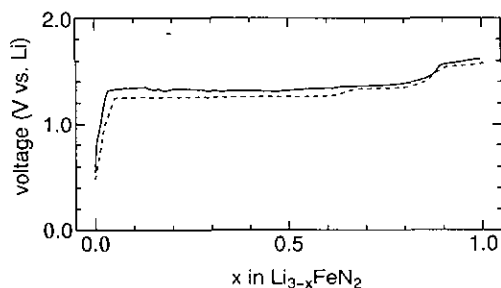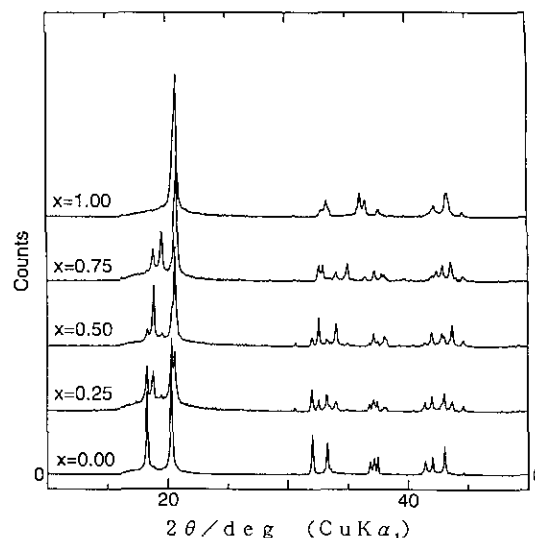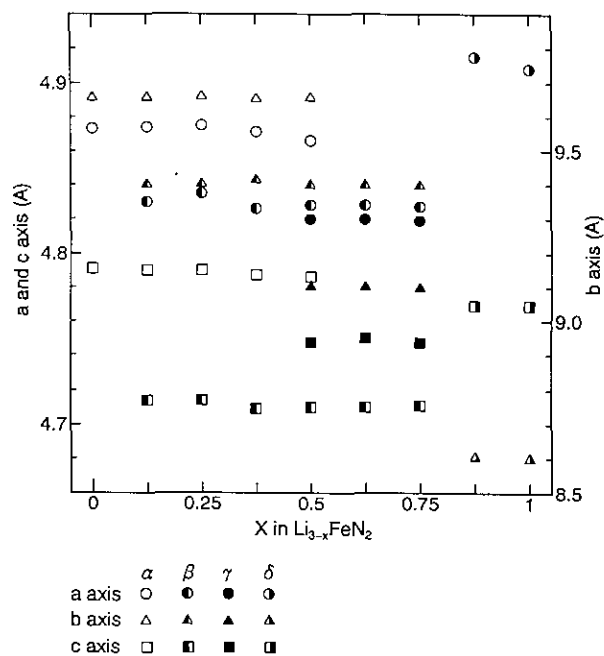

FIG. 3. Open-circuit voltage and closed-circuit voltage of $Li_{3-x}FeN_2$. OCV, dot line; CCV, solid line (150 mA cm^{-2}).

FIG. 5. Variation of the lattice parameters as a function of x in $Li_{3-x}FeN_2$.
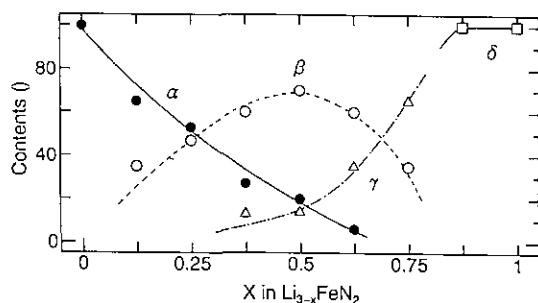
FIG. 6. Composition dependence of phase content for $Li_{3-x}FeN_2$. ●, α phase; ○, β phase; △, γ phase; and □ δ phase.

3. Li Deintercalation and Physical Properties

3.1. Electrical conductivity.

Careful examination of the curves in Fig. 3 shows that the overpotential in $0 \leq x \leq 0.5$ is higher than that in $0.5 \leq x \leq 0.75$. This means that electrical conductivity increases with Li deintercalation. To confirm this, the electrical conductivity at room temperature was measured by a dc four-probe method, using Ni as a blocking electrode. A cathode that was deintercalated without using acetylene-black and Teflon was shaped to form a block 4 × 3 × 10 mm in size. Figure 7 shows the temperature dependence of electrical resistivity for various Li contents. The resistivity clearly decreases with Li deintercalation, indicating an increase of carrier density on deintercalation. All samples remain semiconducting. Though the resistivity is relatively high, no rapid increase at lower temperature is observed. In general, high resistivity and high activation energy go together, while $Li_{3-x}FeN_2$ shows only a slight increase in resistivity at low temperatures. Our samples was not sintered but only compressed; thus, the conducting path
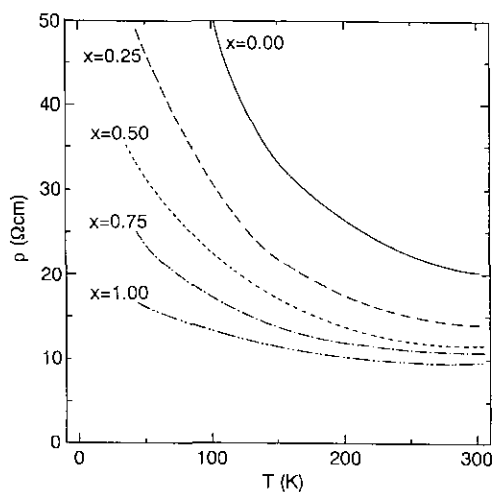

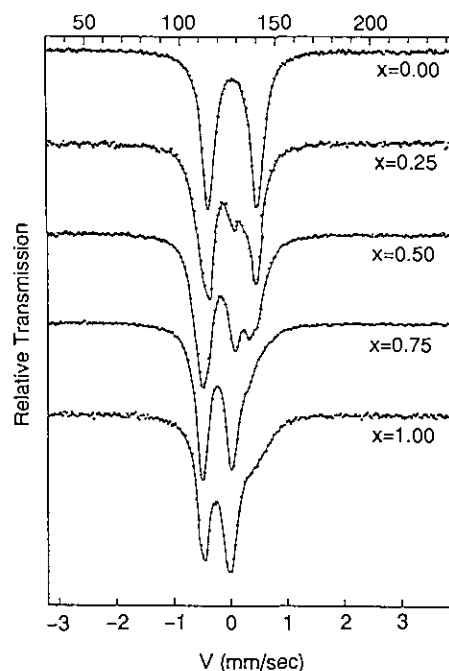FIG. 7. Temperature dependence of apparent electrical resistivity of pressed pellets of $Li_{3-x}FeN_2$.

FIG. 8. Room temperature Mössbauer spectra of Li_3FeN_2.

must be very narrow, being blocked by grain boundaries. The electrical conductivity of $Li_{3-x}FeN_2$ is generally assumed to be quite high. In addition, the small temperature dependence near room temperature makes us expect that the cell performance would not show any troublesome temperature dependence.

3.2. Mössbauer Spectrum.

The Mössbauer spectra of $Li_{3-x}FeN_2$ with various Li contents, measured at room temperature, are shown in Fig. 8, and the isomer shift (IS) and quadrupole splitting (QS) are listed in Table 5. For $x = 0$, a single quadrupole doublet (IS = 0.0525 mm/sec, QS = 0.875 mm/sec) assigned to Fe(III) in low spin state is observed. With increasing x a new doublet with a more negative isomer shift and a smaller quadrupole splitting overlaps, and for $0.75 < x$ it becomes dominant. The shoulder appearing at the right of the quadrupole peak for $0.75 < x$ has yet to be assigned; it may be attributed to the product decomposition brought on overcharge. This suggests that Li deintercalation oxidizes Fe(III) to Fe(IV). The computer peak fittings reveal that each phase has slightly different IS and QS values for Fe(III) and Fe(IV). The magnetic susceptibility measurement of Li_3FeN_2 by Gudat et al. (12) indicated that the Fe(III) ions were in the low spin state. The more negative value of IS (−0.22 mm/sec) for Fe(IV) in Li_2FeN_2 relative to the typical values of −0.0 mm/sec measured for oxides such as $SrFe^{4+}O_3(14)$, $CaFe^{4+}O_3(15)$, etc., is consistent with an assumption that the Fe(IV) state in $Li_{3-x}FeN_2$ is in the low spin state of $d\varepsilon^4\ d\gamma^0$.

NISHIJIMA ET AL.

TABLE 5
Mössbauer Data for $Li_{c-x}FeN_2$

	Fe^{3+} (α phase)			Fe^{3+} (β phase)			Fe^{4+} (β phase)			Fe^{4+} (β phase)			Fe^{4+} (δ phase)		
	IS (mm/sec)	QS (mm/sec)	I (%)	IS (mm/sec)	QS (mm/sec)	I (%)	IS (mm/sec)	QS (mm/sec)	I (%)	IS (mm/sec)	QS (mm/sec)	I (%)	IS (mm/sec)	QS (mm/sec)	I (%)
$x = 0.00$	0.052	0.875	100	—	—	—	—	—	—	—	—	—	—	—	—
$x = 0.24$	0.045	0.826	59	−0.032	0.684	23	−0.249	0.631	18	—	—	—	—	—	—
$x = 0.50$	0.058	0.886	12	−0.041	0.811	44	−0.232	0.619	43	—	—	—	—	—	—
$x = 0.75$	—	—	—	0.079	0.700	22	−0.233	0.621	23	−0.239	0.525	54	—	—	—
$x = 1.00$	—	—	—	—	—	—	—	—	—	—	—	—	−0.240	−0.520	100

3.3. Li Intercalation Reaction. The discharge OCV and CCV curves for the samples charged to $x = 1.0$ are shown in Fig. 9. The potential difference between the charge and the discharge curves is small, indicating a high degree of reversibility. In the XRD pattern of the fully discharged sample, only the original phase (α phase) was seen. Li_3FeN_2 has thus been found to have a high capacity of 260 mA hr g^{-1}.

CONCLUSION

Li_3FeN_2 was easily synthesized from a 3.5:1 mixture of Li_3N and Fe_4N by using a traditional ceramic method in a 1% H_2–99% N_2 stream. Li could be deintercalated, forming $Li_{3-x}FeN_2$ in a range of $0 \le x \le 1.0$. With increasing x, four phases sequentially appeared. The electrical resistivity decreased with increasing x. The OCV and CCV curves for both charge and discharge directions were
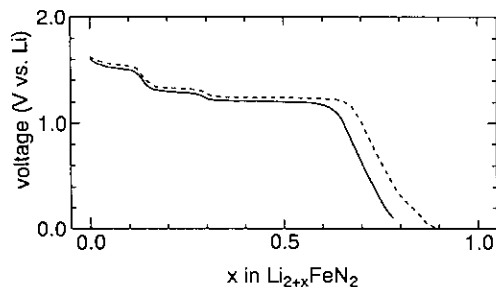
very flat, and the overpotential was very low. Li_3FeN_2 has ideal properties not only as a cathode for Li secondary batteries, but also as an anode if combined with a cathode having high electrode potential relative to lithium metal.

REFERENCES

1. A. Rabenau, *Solid State Ionics* 6, 277 (1982).
2. T. Lapp, S. Skaarup, and A. Hooper, *Solid State Ionics* 11, 97 (1983).
3. P. M. Richards, *J. Solid State Chem.* 33, 127 (1980).
4. R. Juza, H. H. Weber, and E. Meyer-Simon, *Z. Anorg. Allg. Chem.* 48, 273 (1953).
5. R. Juza and F. Hund, *Z. Anorg. Allg. Chem.* 13, 257 (1948).
6. M. Fromont, *Rev. Chim. Miner.* 259, 447 (1967).
7. H. Yamane, S. Kikkawa, H. Horiuchi, and M. Koizumi, *J. Solid State Chem.* 65, 6 (1986).
8. H. Yamane, S. Kikkawa, and M. Koizumi, *J. Solid State Chem.* 71, 1 (1987).
9. H. Yamane, S. Kikkawa, and M. Koizumi, *Solid State Ionics* 15, 51 (1985).
10. H. Yamane, S. Kikkawa, and M. Koizumi, *Solid State Ionics* 25, 183 (1987).
11. R. Juza, E. Anschutz, and H. Puff, *Agnew. Chem.* 71, 161 (1959).
12. A. Gudat, R. Kniep, and A. Rabenau, *J. Less-Common Met.* 161, 31 (1990).
13. F. Izumi, *J. Miner. Soc. Jpn.* 17, 37 (1985).
14. J. B. MacChesney, R. C. Sherwood, and J. F. Potter, *J. Chem. Phys.* 43, 1907 (1965).
15. Y. Takeda, O. Naka, M. Takano, T. Shinjo, T. Takada, and M. Shinada, *Mater. Res. Bull.* 13, 61 (1978).

FIG. 9. OCV and CCV curves of $Li_{3-x}FeN_2$ in discharging. OCV, dot line; CCV, solid line (150 mA cm^{-2}).